ACS NANO

www.acsnano.org

ARTICLE

Crystal Orientation Controlled Photovoltaic Properties of Multilayer GaAs Nanowire Arrays

Ning Han,[*,†,‡] Zai-xing Yang,[§,∥,⊥] Fengyun Wang,[#] SenPo Yip,[§,∥,⊥] Dapan Li,[§,⊥] Tak Fu Hung,[§] Yunfa Chen,[†,‡] and Johnny C. Ho[*,§,∥,⊥]

[†]State Key Laboratory of Multiphase Complex Systems, Institute of Process Engineering, Chinese Academy of Sciences, Beijing, 100190, People's Republic of China

[‡]Center for Excellence in Urban Atmospheric Environment, Institute of Urban Environment, Chinese Academy of Sciences, Xiamen 361021, People's Republic of China

[§]Department of Physics and Materials Science, City University of Hong Kong, Kowloon, Hong Kong, People's Republic of China

[∥]State Key Laboratory of Millimeter Waves, City University of Hong Kong, Kowloon, Hong Kong, People's Republic of China

[⊥]Shenzhen Research Institute, City University of Hong Kong, Shenzhen, 518057, People's Republic of China

[#]Cultivation Base for State Key Laboratory, Qingdao University, Qingdao, 266071, People's Republic of China

Supporting Information

ABSTRACT: **In recent years, despite significant progress in the synthesis, characterization, and integration of various nanowire (NW) material systems, crystal orientation controlled NW growth as well as real-time assessment of their growth−structure−property relationships still presents one of the major challenges in deploying NWs for practical large-scale applications. In this study, we propose, design, and develop a multilayer NW printing scheme for the determination of crystal orientation controlled photovoltaic properties of parallel GaAs NW arrays. By tuning the catalyst thickness and nucleation and growth temperatures in the two-step chemical vapor deposition, crystalline GaAs NWs with uniform, pure ⟨110⟩ and ⟨111⟩ orientations and other mixture ratios can be successfully prepared. Employing lift-off resists, three-layer NW parallel arrays can be easily attained for X-ray diffraction in order to evaluate their growth orientation along with the fabrication of NW parallel array based Schottky photovoltaic devices for the subsequent performance assessment. Notably, the open-circuit voltage of purely ⟨111⟩-oriented NW arrayed cells is far higher than that of ⟨110⟩-oriented NW arrayed counterparts, which can be interpreted by the different surface Fermi level pinning that exists on various NW crystal surface planes due to the different As dangling bond densities. All this indicates the profound effect of NW crystal orientation on physical and chemical properties of GaAs NWs, suggesting the careful NW design considerations for achieving optimal photovoltaic performances. The approach presented here could also serve as a versatile and powerful platform for *in situ* characterization of other NW materials.**

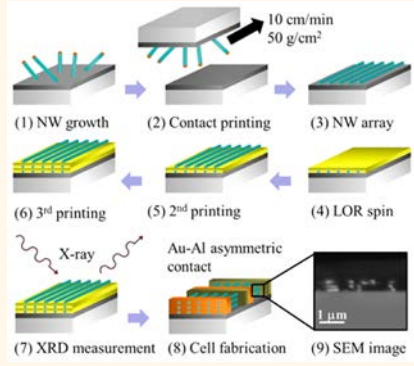

KEYWORDS: *GaAs nanowire, orientation, contact printing, X-ray diffraction, photovoltaic, Schottky contact*

In the past decade, because of their superior electrical and optical properties, one-dimensional (1-D) semiconductor nanostructured materials such as quantum nanowires (NWs) have been vastly explored as fundamental building blocks for electronic, power generation, conversion and storage devices, *etc.* For example, GaAs NWs have been demonstrated with one of the highest theoretical energy conversion efficiencies of >30% for single-junction photovoltaics, which are now extensively investigated for next-generation high-performance and low-cost solar cells owing to their intrinsically direct band gap, optimal gap width (1.42 eV), and high electron mobility (8500 $cm^2\ V^{-1}\ s^{-1}$).[1−8] Specifically, both horizontally and vertically configured single GaAs NW photovoltaic devices, with the core−shell p−i−n junction, have been recently fabricated with an impressively high efficiency of up to 40%,[4,8] illustrating their potency for solar cell utilizations. These 1-D nanomaterials typically originate from the anisotropic properties of semiconductor crystals, in which they can be either constructed with chemically stable crystal planes *via* the "top-down" etching schemes or grown along thermodynamically preferable planes by the "bottom-up" synthesis methods. It is noted that the top-down approaches

Received: April 12, 2016
Accepted: May 25, 2016
Published: May 25, 2016

DOI: 10.1021/acsnano.6b02473
ACS Nano 2016, 10, 6283−6290

often damage the NW surface and restrict the manipulation of NW orientations, which limit their practical deployments. On the other hand, the preferred NW growth directions achieved with bottom-up techniques are usually varied with the NW diameters and their corresponding surface-to-volume ratios, as there are always different interplays between their surface and bulk crystal free energies; therefore, these various NW crystal orientations would induce dramatically different device performances for technological applications. For instance, when designing anodes for Li-ion batteries, Si NWs with ⟨110⟩ surface planes are highly preferred for ion insertion since they are more susceptible to accommodate the larger degree of volume expansion in order to prolong their electrode reliability.[9,10] In heterogeneous catalysis, Co_3O_4 NWs with ⟨110⟩ surface planes are found to exhibit one of the highest CO catalytic properties, which is attributed to the efficient alignment of active Co^{3+} ions on the NW surface during the chemical reaction.[11] However, apart from these studies of structural and chemical properties of NWs, there are very few reports investigating the relationship between NW orientations and their optoelectronic properties, especially since different crystal surfaces are recognized to possess varied recombination centers for the deterioration of the photocurrent extraction.[12,13] As a result, a crystal orientation dependent photovoltaic study is essential for material design, synthesis, and integration of large-scale and highly efficient NW-based photovoltaic systems.

Generally, there are at least two major challenges in assessing and controlling the crystal orientation dependent optoelectronic properties of NWs. One well-known issue is to identity the property changes with the orientation of grown NWs. Although there are several techniques commonly employed to evaluate the NW growth orientation such as high-resolution transmission electron microscopy (HRTEM) or selected area electron diffraction (SAED), it is merely impracticable to subsequently fabricate postcharacterized NWs into devices for detailed electrical and optical measurements and *vice versa*. At the same time, conventional X-ray diffraction is constantly utilized for crystal structure determination, but the dominant growth direction can only be assessed stringently for the vertical NW arrays.[14,15] When individual NWs are lain down horizontally on substrates, the NWs do not contribute sufficient thickness for enough scattering events for the diffraction phenomenon. On the other hand, recently, significant progress has been made in *in situ* microscopic characterization to assess simple nanostructured properties along with the material synthesis and their interaction with others,[16−18] such that *in situ* TEM can now enable direct observation of the NW growth,[19,20] NW deformation under strain,[21,22] Si nanoparticle interactions with Li-ions,[23] *etc*. However, to date, all these *in situ* measurements still cannot reveal complex material or device characteristics, including crystallographic anisotropy, photovoltaic output, and carrier mobility, all of which are important parameters for the development of high-efficiency solar cells. Even though electron beam induced current (EBIC) and spatial photocurrent microscopic measurements can be employed to directly extract the minority diffusion length, a key factor determining the effective accumulation of the photocurrent,[24,25] no corresponding NW orientation information can be obtained here. Another key challenge comes in the controllable synthesis of "bottom-up" NWs with manipulable and uniform properties in the large scale. In the epitaxial NW growth, most NWs would prefer to grow along the close-packed planes with the lowest crystal energy in the ⟨111⟩ directions, independent of the underlying crystalline substrates employed.[26−28] Even if the metastable crystal structure or growth orientation of NWs can be obtained by tailoring the processing conditions,[29−31] it is still difficult to attain uniform properties of NWs, as their properties (*e.g.*, growth orientation) can be easily affected by the catalyst choice, diameters, *etc*. It is well known that Si and ZnSe NWs with ultrasmall diameters are predominately grown along the ⟨110⟩ directions, while their thick counterparts preferably grow along the ⟨111⟩ orientations due to the interchange between their surface and bulk energies.[32−34] In most cases, the obtained NW orientations are not uniform, which deters their placement for the scale-up practical exploitations.

In this work, we propose, design, and develop a multilayer NW printing scheme for the determination of crystal orientation controlled photovoltaic properties of parallel GaAs NW arrays. By tuning the catalyst thickness and nucleation and growth temperatures in the two-step chemical vapor deposition (CVD) growth, GaAs NWs with uniform, pure ⟨110⟩ and ⟨111⟩ orientations and other mixture ratios have been successfully obtained. High-density parallel NW arrays can then be configured by multilayer printing on substrates to yield high-intensity XRD characteristic peaks for crystal orientation assessment, followed by the device fabrication, in order to evaluate their corresponding photovoltaic performances. When constructed into simple Schottky NW solar devices, it is found that the ⟨111⟩-oriented GaAs NWs result in a higher open-circuit voltage by ∼0.21 eV as compared with that of ⟨110⟩ NWs, which can be interpreted by the different surface Fermi level pinning effects of the varied {110} and {111} NW sidewalls due to the altered surface As dangling bond densities. All these findings would provide essential information on the relationship between NW orientations and their photovoltaic properties and, more importantly, enable a valuable platform to understand the growth−structure−property relationships of NW material systems for practical utilizations.

Here, we design and establish a multilayer NW printing technique to obtain highly dense NW parallel arrays for the simultaneous and direct determination of the NW orientation by XRD as well as the photovoltaic performance of the subsequently fabricated Schottky NW solar devices. As schematically illustrated in Figure 1, the GaAs NWs grown on amorphous substrates, with unknown growth orientation, are printed onto Si/SiO_2 wafers (50 nm thick thermally grown oxide) to obtain the first NW parallel-arrayed layer *via* contact printing at a velocity of 10 cm/min and a pressure of 50 g/cm^2 (steps 1−3). The LOR 3A lift-off resist (250 nm thick) is next spin-coated onto the fabricated NW arrayed layer at 4000 rpm for 60 s (step 4), and the second and third NW printing steps are performed repeatedly in order to achieve the three-layer GaAs NW arrays (steps 5 and 6). It is noted that lift-off resists are utilized here since they are not photosensitive, but still allow efficient patterning under UV lithography. This way, the multilayer NW arrays can then undergo conventional XRD measurements, followed by the typical device fabrication of Schottky asymmetric Au−Al contacted NW solar cells (steps 7 and 8). The cross-sectional SEM image can confirm the effective stacking of multiple NW parallel-arrayed layers (step 9), demonstrating the advantages of this simple process to construct thick and high-density NW parallel arrays, which facilitate the stimulation of sufficient XRD signals. Eventually, the corresponding photovoltaic performance can be measured

DOI: 10.1021/acsnano.6b02473
ACS Nano 2016, 10, 6283−6290

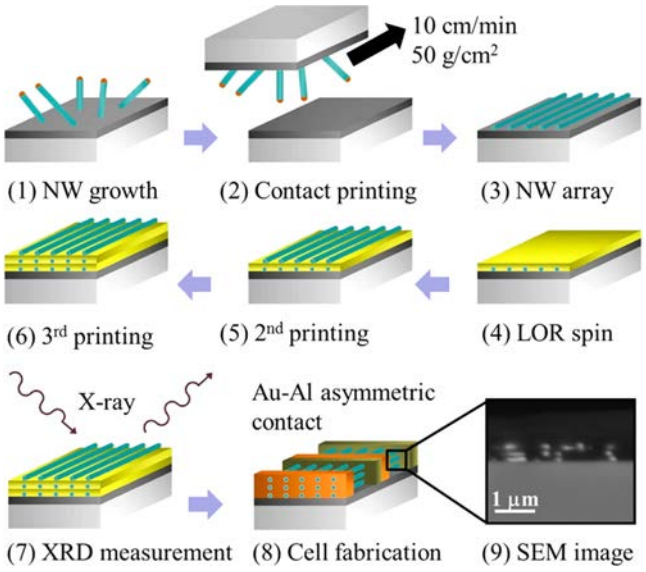

Figure 1. Schematics of the successive NW printing to obtain thick and high-density GaAs multilayer NW arrays for the simultaneous assessment of both NW orientation and their corresponding photovoltaic outputs. It is noted that the unique properties of LOR resists can enable the formation of multilayer NW parallel arrays, ensure the chemical and thermal stability during the ambient and X-ray exposure, and allow the subsequent patterning in the device fabrication. As a result, the same LOR resists can be carried out along the entire fabrication process.

and correlated to the obtained information on NW orientation beforehand.

It is well known that the growth orientation of vertical NW arrays can be easily resolved by XRD with their characteristic peaks. For instance, among many explorations, most vertical ZnO NW arrays are identified to grow along the most thermodynamically stable directions of ⟨0001⟩.[14,15] At this point, we employ a quantitative method to evaluate the growth orientation of parallel NW arrays based on the characteristic peaks of their sidewalls. Specifically for GaAs NWs, the cubic zinc-blende (ZB) crystal structure is the lowest energy stable phase when the diameter is larger than 10−20 nm,[30,35,36] with two dominant intense peaks of (111) and (220) in the XRD pattern with a typical intensity ratio of 100:60 to 100:50, as shown in Table 1 (PDF 3-65-234 and 32-0389). In powder XRD, the intensity of each (*hkl*) plane can be simply expressed

Table 1. Crystal Plane Multiplicity (*M*) and Relative XRD Peak Intensity (*I*) of the GaAs Powders (PDF 3-65-234 and 32-0389) and NWs along the ⟨111⟩ and ⟨110⟩ Orientations

	M_{111}	M_{220}	growth condition	I_{111}:I_{220}
powder[a]	8	12		100:60(50)[c]
⟨111⟩ NW[a]	0	6		0:100
⟨110⟩ NW[a]	4	2		100:20(17)
⟨111⟩:⟨110⟩ = 1:0[b]			6 nm Au, 650/610 °C	0:100
0:1[b]			12 nm Au, 670/630 °C	100:18
3.9(4.8):1[b]			12 nm Au, 650/600 °C	39:100
1.9(2.4):1[b]			12 nm Au, 660/620 °C	74:100

[a]These rows give the theoretical values. [b]These rows display the measured values and extracted mixing ratio of ⟨111⟩- and ⟨110⟩-oriented NW orientations. [c]Values in parentheses refer to the calculation based on I_{111}:I_{220} being 100:50.

as $I_{hkl} = KM_{hkl}$, where K is a constant related to the instrument, angle of diffraction, *etc.*, and M_{hkl} is the plane multiplicity (see Supporting Information for more details). In general, the {111} family has eight equivalent planes (*i.e.*, $M_{111} = 8$), while the {220} family has 12 equivalent ones (*i.e.*, $M_{220} = 12$) for powder samples in XRD measurements. However, the multiplicity would change accordingly in the case of parallel NW arrays because there are only fractions of these equivalent planes taking part in the XRD characterization due to their horizontal geometries. As depicted in Figure 2a, when considering the

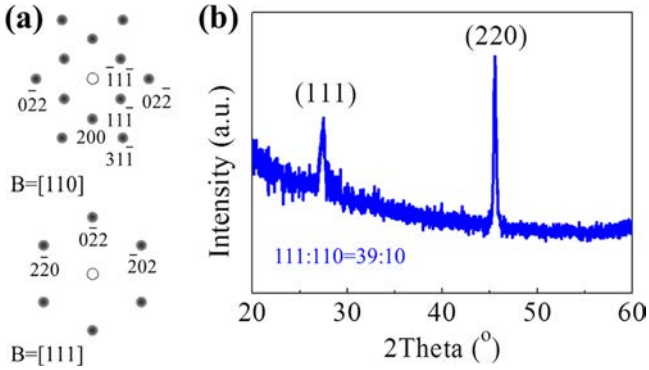

Figure 2. Illustrative example of the NW orientation determined by XRD. (a) Schematics of the plane multiplicity calculation from electron diffraction patterns of ⟨110⟩ and ⟨111⟩ zones. Using the [110]-oriented NW as an example, only $(1\bar{1}\bar{1})$, $(\bar{1}\bar{1}1)$, $(1\bar{1}1)$, and $(\bar{1}1\bar{1})$ planes can participate in the diffraction, while the other (111), $(\bar{1}\bar{1}\bar{1})$, $(\bar{1}11)$, and $(1\bar{1}\bar{1})$ planes give insignificant signals (see details in Supporting Information Figure S1); therefore, the multiplicity of {111} planes is determined as 4 for ⟨110⟩-oriented NWs. Similarly, the multiplicity of {110} planes is determined as 6 for ⟨111⟩-oriented NWs. (b) Typical XRD pattern collected for the assembled three-layer NW arrays. From the peak intensity analysis, the mixing ratio of ⟨111⟩- and ⟨110⟩-oriented NWs would be equal to 3.9:1.

⟨110⟩-oriented NWs, there are only four (111) and two (220) equivalent planes participating in the diffraction, and thus the multiplicity values of M_{111} and M_{220} turn into 4 and 2, respectively. Likewise, the multiplicity values of M_{111} and M_{220} become 0 and 6, consequently, for the ⟨111⟩-oriented NWs. These varied multiplicity values would induce different peak intensities in their corresponding XRD patterns such that the pure horizontal ⟨111⟩-oriented NW arrays will only have the (220) peak, while ⟨110⟩-oriented NW arrays will have both (111) and (220) peaks with intensities of I_{111}:I_{220} being 100/2:60/6 (*i.e.*, 100:20), as derived from the powder XRD. In this case, information about the NW orientation can be extracted by decoupling the characteristic peak intensities of (111) and (220) planes in the GaAs NW arrays in order to determine the mixing ratio of ⟨111⟩ and ⟨110⟩ directions.

RESULTS AND DISCUSSION

As a proof-of-concept, in order to demonstrate the NW orientation determination by the above-mentioned characteristic XRD peak intensity analysis, we collect the XRD pattern of three-layer GaAs NW arrays synthesized in our previously reported two-step growth condition of "650/600" as given in Figure 2b (see the Methods section for the growth details).[37] These temperature values indicate the NW nucleation and growth temperatures employed, respectively. From the peak intensity analysis, the relative intensity of I_{111}:I_{220} is 39:100,

DOI: 10.1021/acsnano.6b02473
ACS Nano 2016, 10, 6283−6290

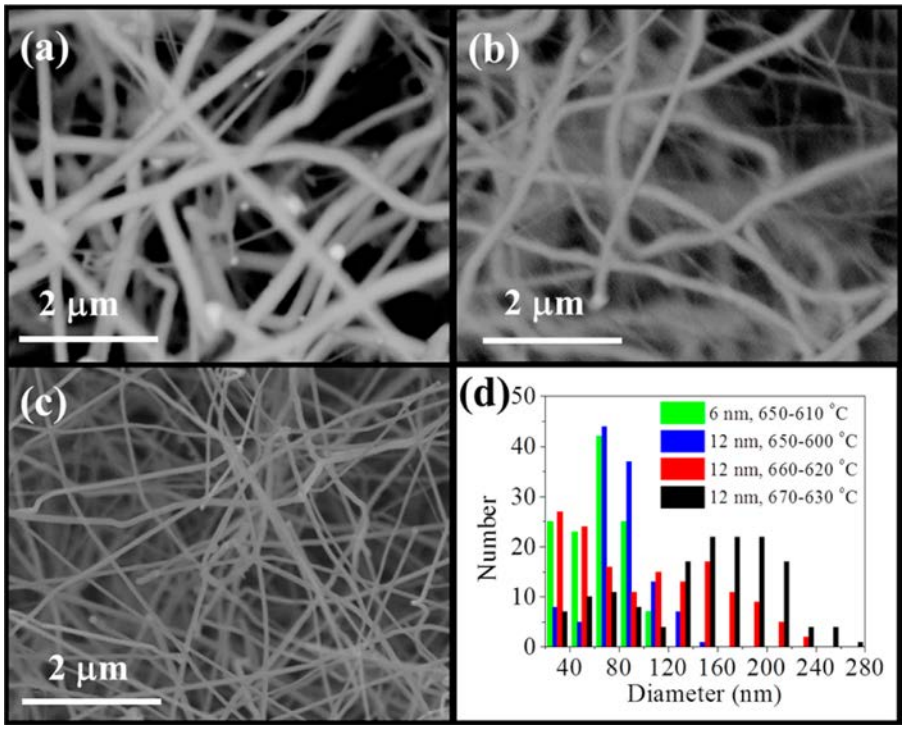

Figure 3. SEM images and diameter statistics of the GaAs NWs grown by the two-step CVD method: (a) 12 nm thick Au catalyst film with growth temperatures of 670/630 °C, (b) 12 nm thick Au catalyst film with growth temperatures of 660/620 °C, (c) 6 nm thick Au catalyst film with growth temperatures of 650/610 °C, and (d) diameter histogram of the grown NWs.

with the (111) peak attributable to ⟨110⟩-oriented NWs and the (220) peak to both ⟨111⟩- and ⟨110⟩-oriented NWs along with the corresponding contribution of (100 − 39/5) = 92.2 and 39/5 = 7.8, respectively. Combined with the multiplicity of the (220) planes, it is determined that the mixing ratio of ⟨111⟩- and ⟨110⟩-oriented NWs would equal 92.2/6:7.8/2, that is 3.9:1. This estimated ratio is perfectly consistent with our formerly compiled NW statistics of actually measuring the individual NW orientation by SAED with the ratio of ⟨111⟩:⟨110⟩ being 10:3.[37] Moreover, since the X-ray beam size is relatively large, being on the order of millimeters in diameters, a large amount of NWs can then be sampled in this study for the representative assessment of their corresponding orientation. Also, the peak intensity predominantly comes from ⟨111⟩- and ⟨110⟩-oriented NWs, as there are not any ⟨211⟩- and ⟨311⟩-oriented NWs obtained in this two-step growth; therefore, only (111) and (220) peaks are observed in the XRD performed in this work. It should be as well noted that there may be a complication in determining the peak intensity, which is highly dependent on the NW placement, especially its tilting angle with respect to the vertical direction after the NW printing. As depicted in Supporting Information Figure S1, the ⟨110⟩- and ⟨111⟩-oriented NWs would have to tilt with the angles of 54.7° and 19.5°, respectively, in order to make their (111) planes not participate in the XRD process and to contribute errors to the peak intensity analysis. In other words, for NWs with a length of 10 μm, they have to rest on the steps with heights of 8.2 and 3.3 μm, accordingly; however, this is not realistic in our current NW printing setup since the LOR 3A layer is only 250 nm thick and the total thickness of the three-layer NW arrays is less than 1 μm. In addition, although the multiplicity value is also affected by the random location of the NWs, there is a significant amount of NWs in this parallel array configuration, contributing to the sufficient XRD signal and precise multiplicity values (see Supporting Information for more details). These complementary theoretical analyses as well as experimental data have illustrated the practicability and accurateness of this NW orientation identification *via* the XRD peak intensity analysis.

After the peak intensity analysis method has been validated in assessing the NW orientation, the growth conditions can then be tailored in order to synthesize GaAs NWs with various orientations in different controllable ratios. As reported in the past, during the two-step NW growth, the initial high-temperature nucleation step plays an important role in controlling the obtained NW diameter distribution, length, orientation, and crystal defect density. All this can be attributed to the Gibbs−Thomson effect governed by the equation $\ln(C_d/C_0) = 4\gamma V_m/(dRT)$, where C_d is the concentration of Ga in Au nanoparticles with the diameter of d, C_0 is the equilibrium concentration in flat surface ($d \rightarrow \infty$) materials, γ is the surface energy, V_m is the molar volume of Au, R is a constant (8.314 J mol^{-1} K^{-1}), and T is the temperature. After compensation of the positive contribution of larger γ and V_m at higher temperature and negative contribution of T with different Au catalyst diameters, different Ga solubilities can be obtained.[37,38] Specifically, a higher solubility would lead to the faster Ga precursor diffusion into the growth front (*i.e.*, the catalyst/NW interface), inducing a higher NW growth rate, and hence results in the varied growth orientations in accordance with the precursor concentration effects as described in the literature.[39,40] In this work, we adjust the temperature profile systemically with the aim to tailor different Au−Ga ratios in the catalyst seeds of different diameter groups and then to guide the subsequent NW growth along controllable orientations *via* the manipulation of catalytic composition. In general, the NWs grown by lower temperatures (*i.e.*, less than 650/610 °C) would have a morphology similar to that reported in our

DOI: 10.1021/acsnano.6b02473
ACS Nano 2016, 10, 6283−6290

previous studies. When the temperature is increased to 660/620 °C and 670/630 °C, the NWs would become thicker in their diameters and larger in their diameter distributions, as depicted in the SEM images in Figure 3a and b. At the same time, once the thinner catalyst film (*e.g.*, 6 nm Au) is employed in the NW growth conditions of 650/610 °C, a thinner diameter and narrower diameter distribution are obtained, as shown in Figure 3c. All the NW diameter distributions are estimated based on the statistics of more than 100 individual NWs, with the histograms illustrated in Figure 3d. The significant diameter distribution would lead to a potential NW orientation inhomogeneity, as reported in the literature.

Typically, as demonstrated in Figure 4a and b, the relatively thin GaAs NWs with diameters of around 100 nm would grow along the ⟨111⟩ directions, while the thicker ones would grow along the ⟨110⟩ directions. This finding is in perfect agreement with our previous studies that show that the small-diameter Au catalysts usually have a higher Ga solubility as well as a larger Ga diffusive velocity for the NW growth along the close-packed (111) planes, while the slower Ga diffusion in the large-diameter catalysts and catalysts with a lower Ga content would lead to growth along the (220) planes.[38] However, due to the significant NW diameter distribution, one cannot distinguish a clear threshold to estimate the orientation profiles simply based on their diameter distribution. On the other hand, after the NWs are contact-printed into the three-layer parallel arrays as described above, XRD measurements and the peak intensity analysis can be performed easily in order to identify the NW orientation, even with a mixed ratio of ⟨111⟩:⟨110⟩ directions being 0:1, 3.9:1, 1.9:1, and 1:0, respectively, for the NWs grown by 12 nm Au at 670/630 °C, 660/620 °C, and 650/600 °C and 6 nm Au at 650/610 °C, as compiled in Table 1. It is obvious that by manipulating the process conditions such as the Au film thickness and growth temperatures, the NW diameter and growth orientation can be precisely controlled to yield uniform NWs of ⟨111⟩, ⟨110⟩, or mixed orientations.

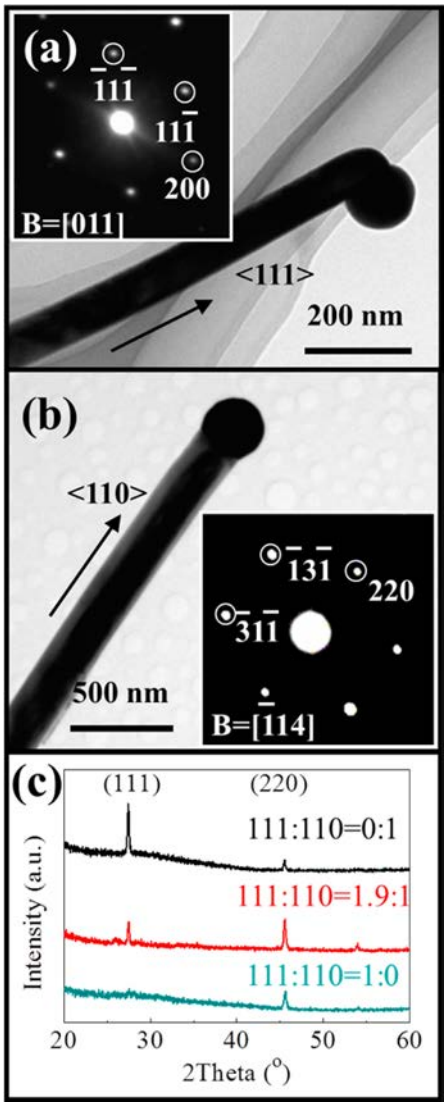

Figure 4. Growth orientation determination by SAED and XRD. (a) Typical thin NWs grown along the ⟨111⟩ directions, (b) thick NWs grown along the ⟨110⟩ directions, and (c) XRD patterns collected of the three-layer GaAs NW parallel arrays achieved by three consecutive contact printings.

Once the NW orientation is perfectly controlled, characterized, and confirmed, it is important to evaluate the orientation effect on the photovoltaic properties of GaAs NWs. In this case, simple Schottky structured solar cells employing the three-layer NW parallel arrays can be fabricated with asymmetric Au−Al contacts. Figure 5a gives the device schematic and the corresponding electronic band diagram illustrating its operating principle with Schottky contacts.[41] As depicted in Figure 5b, it is evident that the obtained NW arrays have a high density of more than 5 NWs/μm due to the three layers of NW printing, which can be clearly observed and verified in the cross-sectional SEM image (Supporting Information Figure S2). More importantly, nine individual single cells can be readily connected in the tandem or series configuration by conventional photolithography, in which the photovoltaic output can be reinforced, while the cell-to-cell variation can be minimized. Figure 5c demonstrates the corresponding photovoltaic performance. It shows clearly that the higher open-circuit voltages (V_{oc}) are attained for the devices with greater fractions of NWs oriented in the ⟨111⟩ directions. Specifically, the purely ⟨111⟩-oriented GaAs NW arrays are found to have a V_{oc} of 3.0/9 = 0.33 V for the individual cell, whereas the ⟨110⟩-oriented ones have a much smaller V_{oc} of only 1.1/9 = 0.12 V, indicating the significant NW orientation effect on their photovoltaic output. These V_{oc} values are slightly lower than those of the bulk and p−i−n structured cells,[4,12,13] as it is well known that the III−V nanomaterials, especially the NWs, possess a high surface-to-volume ratio with abundant surface states, which would result in severe surface recombination and surface Fermi level pinning. Although there is a large work function difference of around 1.0 eV between the two contact electrodes (*i.e.*, Au ≈ 5.3 eV and Al ≈ 4.3 eV),[42] the Fermi level pinning still exists but is relaxed, accounting for the much smaller V_{oc} of 0.12 to 0.33 eV observed here. Furthermore, more than 20 single NW solar devices with controlled growth orientations and the same cell structure are also fabricated and characterized, in which similar results are perceived, further confirming the effect of Fermi level pinning on NWs observed in this work.

To further shed light on the originality of different V_{oc}'s observed in different NW orientations, the contact properties of grown NWs are then investigated in detail. Since different crystal surface planes consist of varied atomic arrangements, and hence contribute to different types of surface states, this might result in a key factor influencing the Schottky barrier

DOI: 10.1021/acsnano.6b02473
ACS Nano 2016, 10, 6283−6290

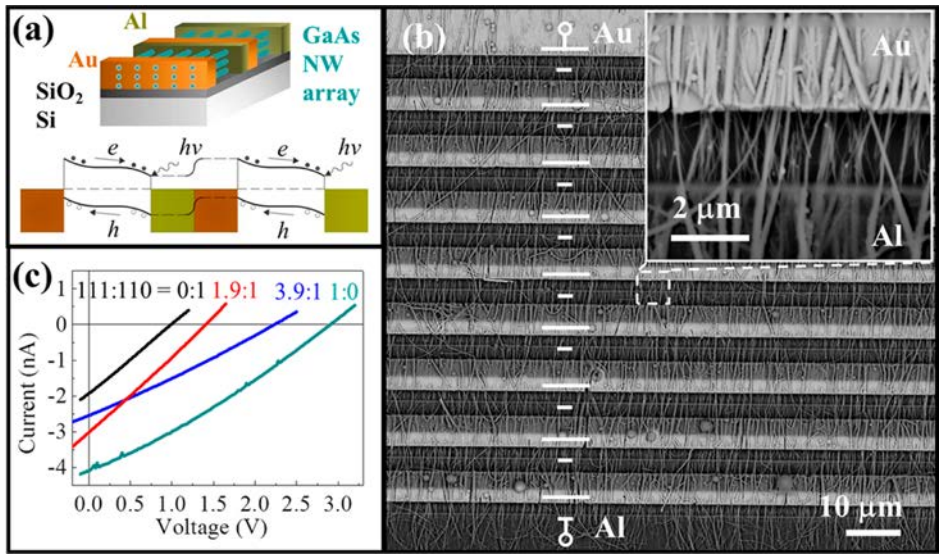

Figure 5. GaAs NW arrayed Schottky solar cells. (a) Schematic of the device structure and its corresponding electronic band diagram, (b) SEM images with the illustrative schematic of nine individual cells connected in series, and (c) output performances of the cells fabricated with different mixing ratios of ⟨111⟩- and ⟨110⟩-oriented NWs.

height when the NWs contact metal electrodes. Typically, surface states originate from dangling bonds of the group V component on the III−V semiconductor surface; therefore, characteristics of different As dangling bonds on various crystal planes should be considered.[1,8,43,44] As illustrated in the approximate atomic model of GaAs NWs in Figure 6, ⟨111⟩-oriented NWs contain six {110} surface planes, while ⟨110⟩-oriented NWs are surrounded by two {100} and four {111} surface planes. The {110} planes are composed of one Ga and one As dangling bond (DB) per unit cell (*i.e.*, 0.4 × 0.565 nm in Figure 6a), yielding an As dangling bond density of 4.4 DBs/nm^2. On the other hand, due to the polar configuration among {100}, {111}A, and {111}B planes, the As dangling bond density varies from 7.2 (Figure 6b), to 12.5 (Figure S3a), all the way to 21.6 DBs/nm^2 (Figure S3b), accordingly, accounting for an average of 13.8 DBs/nm^2, being ~3 times higher than that of the {110} planes. This way, the minimized As dangling bond density might contribute prominently to attenuation of the surface Fermi level pinning of the ⟨111⟩-oriented NWs and thus leading to the higher V_{oc} of the fabricated Schottky solar cells. In the meanwhile, the lower As dangling bond density would also lead to the alleviated surface recombination of photogenerated electron/hole pairs, contributing to the relatively higher short-circuit current observed in the ⟨111⟩-oriented NWs. All these results indicate the profound effect of NW crystal orientation on physical and chemical properties of GaAs NWs, which suggests the careful NW design consideration for achieving optimal photovoltaic performances. Furthermore, by adapting conventional XRD, multilayer NW printing, and photolithography, a unique, valuable, and *in situ* technology platform has been enabled to evaluate the growth−structure−property relationships of NW materials for practical applications.

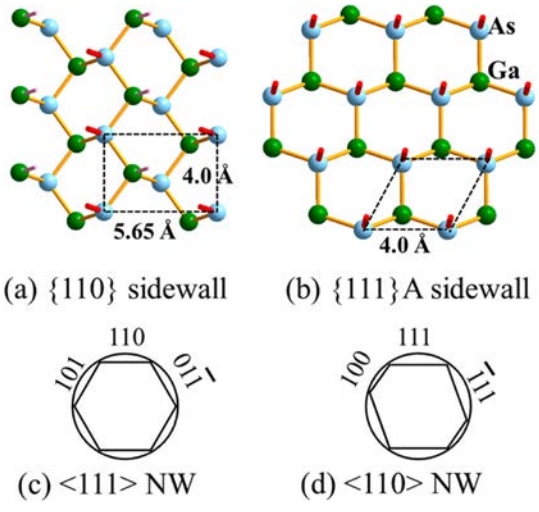

Figure 6. Approximate atomic models of ⟨111⟩- and ⟨110⟩-oriented GaAs NWs. Surface atomic arrangement and illustration of As dangling bonds of (a) {110} NW sidewalls and (b) {111}A NW sidewalls. Demonstration of various surface planes of (c) ⟨111⟩- and (d) ⟨110⟩-oriented NWs.

CONCLUSIONS

In summary, by tuning the catalyst thickness as well as the nucleation and growth temperatures of the two-step growth process, crystalline and uniform GaAs NWs with controllable growth orientation can be successfully obtained in the solid-source chemical vapor deposition system. Specifically, the NW growth orientation can be assessed from the characteristic peak intensity of XRD patterns collected after the NWs have been contact-printed into multilayer parallel arrays assisted by the use of the LOR resist. This *in situ* XRD characterization can enable the real-time NW orientation determination along with the subsequent fabrication of NW parallel array based Schottky photovoltaic devices. It is found that the open-circuit voltage of purely ⟨111⟩-oriented NW arrayed devices is far higher than that of ⟨110⟩-oriented NW arrayed counterparts, which can be interpreted by the different surface Fermi level pinning existing on various NW crystal surface planes due to the different As dangling bond densities. All these results indicate the significant effect of NW orientation on the photovoltaic performance, suggesting the technological potency of employing these purely

DOI: 10.1021/acsnano.6b02473
ACS Nano 2016, 10, 6283−6290

⟨111⟩-oriented GaAs NWs for low-cost, high-performance solar cells. In the future, this versatile, effective, and *in situ* characterization platform can be utilized to systematically study the orientation and other complementary structural effects on device properties of other NW material systems.

METHODS

GaAs NW Growth and Characterization. The GaAs NWs are synthesized in a solid-source chemical vapor deposition system utilizing a two-step growth method with GaAs powders (0.8 g, 99.999% purity) and Au films (6 and 12 nm) as the solid source and the catalyst, respectively, as previously reported.[37,45] In brief, the GaAs powders are held in a boron nitride crucible located in the upstream zone, and the Au catalyst film, thermally predeposited onto Si/SiO_2 substrate pieces (50 nm thick thermally grown oxide, sample size being 5 × 1 cm), is placed in the downstream zone of a two-zone furnace. After pumping down to ∼2 mTorr, H_2 (99.99% purity, flow at 100 sccm) is introduced into the system and the pressure is maintained at ∼0.5 Torr. The Au catalyst is first annealed into nanoparticles at 800 °C for 10 min, cooled, and kept at 650 °C; then the GaAs powder zone begins to ramp up to 860 °C at a rate of 80 °C/min. After a 5 min nucleation step of the Au catalyst at 650 °C, the substrate zone is cooled to the growth temperature of 600 °C. After 60 min of growth, the system is cooled to room temperature in a H_2 atmosphere. NWs can now be harvested and are denoted by the temperatures of the two-step process as "650/600 °C". Similarly, GaAs NWs grown at conditions of "660/620 °C" and "670/630 °C" are also obtained.

The morphology of NWs is observed by a scanning electron microscope (SEM, FEI/Philips XL30) and a transmission electron microscope (TEM, Philips CM20). The corresponding crystal structure is analyzed by using XRD recorded on a Philips powder diffractometer (40 kV, 30 mA) with Cu Kα radiation (λ = 0.154 nm) at steps of 0.02° as well as SAED imaged with TEM (CM20).

Schottky NW Solar Cell Fabrication and Performance Measurement. The multilayer GaAs NW arrays are fabricated by NW contact printing as schematically illustrated in Figure 1. It is worth noticing that the spun LOR resist employed in step 4 should not be soft-baked or performed with any high-temperature step in order to provide sufficient adhesion for the NW printing. Once it reaches step 5, the LOR resist needs a soft-baking step at 150 °C for 10 min after the NW printing; otherwise the subsequently spun LOR resist layer would destroy the alignment of the printed NW arrays. In step 8, the Schottky NW solar cell is fabricated by two successive photolithography steps to define the asymmetric contact electrodes of Au and Al. The Au Schottky electrode layer is first defined by a SUSS MA6 aligner using the LOR 3A lift-off resist/AZ5206 photoresist stack, and then the metal electrode (150 nm thick) can be obtained by thermal evaporation and a subsequent lift-off process. In the same way, the second Al electrode (300 nm thick) can be made by a repeated procedure of photolithography, metal deposition, and lift-off processes. The solar cell performance is measured using a semiconductor analyzer (Agilent 4155C) and a standard probe station under illumination of a solar simulator (Newport 96000).

ASSOCIATED CONTENT

Supporting Information

The Supporting Information is available free of charge on the ACS Publications website at DOI: 10.1021/acsnano.6b02473.

Calculation of XRD peak intensity, error analysis for aligned NWs, cross-sectional SEM image of multilayered GaAs NW array solar cell, and dangling bonds of As in GaAs sidewalls (PDF)

AUTHOR INFORMATION

Corresponding Authors

*E-mail: nhan@ipe.ac.cn.

*E-mail: johnnyho@cityu.edu.hk.

Notes

The authors declare no competing financial interest.

ACKNOWLEDGMENTS

This research was financially supported by the General Research Fund of the Research Grants Council of Hong Kong SAR, China (CityU 11213115), the National Natural Science Foundation of China (Grants 61504151 and 51402160), the State Key Laboratory of Multiphase Complex Systems (MPCS-2014-C-01), the Applied Basic Research Foundation of Qingdao City (Grant 14-2-4-45-jch), the Science Technology and Innovation Committee of Shenzhen Municipality (Grant JCYJ20140419115507588), and a grant from the Shenzhen Research Institute, City University of Hong Kong.

REFERENCES

(1) del Alamo, J. A. Nanometre-Scale Electronics with III-V Compound Semiconductors. *Nature* **2011**, *479*, 317−323.

(2) Goetzberger, A.; Hebling, C.; Schock, H.-W. Photovoltaic Materials, History, Status and Outlook. *Mater. Sci. Eng., R* **2003**, *40*, 1−46.

(3) LaPierre, R. R.; Chia, A. C. E.; Gibson, S. J.; Haapamaki, C. M.; Boulanger, J.; Yee, R.; Kuyanov, P.; Zhang, J.; Tajik, N.; Jewell, N.; Rahman, K. M. A. III-V Nanowire Photovoltaics: Review of Design for High Efficiency. *Phys. Status Solidi RRL* **2013**, *7*, 815−830.

(4) Krogstrup, P.; Jorgensen, H. I.; Heiss, M.; Demichel, O.; Holm, J. V.; Aagesen, M.; Nygard, J.; Morral, A. F. I. Single-Nanowire Solar Cells Beyond the Shockley-Queisser Limit. *Nat. Photonics* **2013**, *7*, 306−310.

(5) Han, N.; Wang, F.; Yip, S.; Hou, J. J.; Xiu, F.; Shi, X.; Hui, A. T.; Hung, T.; Ho, J. C. GaAs Nanowire Schottky Barrier Photovoltaics Utilizing Au-Ga Alloy Catalytic Tips. *Appl. Phys. Lett.* **2012**, *101*, 013105.

(6) Czaban, J. A.; Thompson, D. A.; LaPierre, R. R. GaAs Core−Shell Nanowires for Photovoltaic Applications. *Nano Lett.* **2008**, *9*, 148−154.

(7) Mariani, G.; Scofield, A. C.; Hung, C. H.; Huffaker, D. L. GaAs Nanopillar-Array Solar Cells Employing *in situ* Surface Passivation. *Nat. Commun.* **2013**, *4*, 1497.

(8) Holm, J. V.; Jorgensen, H. I.; Krogstrup, P.; Nygard, J.; Liu, H. Y.; Aagesen, M. Surface-Passivated GaAsP Single-Nanowire Solar Cells Exceeding 10% Efficiency Grown on Silicon. *Nat. Commun.* **2013**, *4*, 1498.

(9) Lee, S. W.; McDowell, M. T.; Choi, J. W.; Cui, Y. Anomalous Shape Changes of Silicon Nanopillars by Electrochemical Lithiation. *Nano Lett.* **2011**, *11*, 3034−3039.

(10) Liu, X. H.; Wang, J. W.; Huang, S.; Fan, F. F.; Huang, X.; Liu, Y.; Krylyuk, S.; Yoo, J.; Dayeh, S. A.; Davydov, A. V.; Mao, S. X.; Picraux, S. T.; Zhang, S. L.; Li, J.; Zhu, T.; Huang, J. Y. *In situ* Atomic-Scale Imaging of Electrochemical Lithiation in Silicon. *Nat. Nanotechnol.* **2012**, *7*, 749−756.

(11) Xie, X. W.; Li, Y.; Liu, Z. Q.; Haruta, M.; Shen, W. J. Low-Temperature Oxidation of Co Catalysed by Co_3O_4 Nanorods. *Nature* **2009**, *458*, 746−749.

(12) Wang, H. P.; Lin, T. Y.; Tsai, M. L.; Tu, W. C.; Huang, M. Y.; Liu, C. W.; Chueh, Y. L.; He, J. H. Toward Efficient and Omnidirectional N-Type Si Solar Cells: Concurrent Improvement in Optical and Electrical Characteristics by Employing Microscale Hierarchical Structures. *ACS Nano* **2014**, *8*, 2959−2969.

(13) Wang, H. P.; Lin, T. Y.; Hsu, C. W.; Tsai, M. L.; Huang, C. H.; Wei, W. R.; Huang, M. Y.; Chien, Y. J.; Yang, P. C.; Liu, C. W.; Chou, L. J.; He, J. H. Realizing High-Efficiency Omnidirectional N-Type Si Solar Cells *via* the Hierarchical Architecture Concept with Radial Junctions. *ACS Nano* **2013**, *7*, 9325−9335.

(14) Tseng, Y. K.; Huang, C. J.; Cheng, H. M.; Lin, I. N.; Liu, K. S.; Chen, I. C. Characterization and Field-Emission Properties of Needle-

DOI: 10.1021/acsnano.6b02473
ACS Nano 2016, 10, 6283−6290

Like Zinc Oxide Nanowires Grown Vertically on Conductive Zinc Oxide Films. *Adv. Funct. Mater.* **2003**, *13*, 811−814.
(15) Wu, W. B.; Hu, G. D.; Cui, S. G.; Zhou, Y.; Wu, H. T. Epitaxy of Vertical ZnO Nanorod Arrays on Highly (001)-Oriented ZnO Seed Monolayer by a Hydrothermal Route. *Cryst. Growth Des.* **2008**, *8*, 4014−4020.
(16) Zhao, M.-H.; Wang, Z.-L.; Mao, S. X. Piezoelectric Characterization of Individual Zinc Oxide Nanobelt Probed by Piezoresponse Force Microscope. *Nano Lett.* **2004**, *4*, 587−590.
(17) Song, J.; Zhou, J.; Wang, Z. L. Piezoelectric and Semiconducting Coupled Power Generating Process of a Single Zno Belt/Wire. A Technology for Harvesting Electricity from the Environment. *Nano Lett.* **2006**, *6*, 1656−1662.
(18) Wang, Z. L.; Song, J. H. Piezoelectric Nanogenerators Based on Zinc Oxide Nanowire Arrays. *Science* **2006**, *312*, 242−246.
(19) Kodambaka, S.; Tersoff, J.; Reuter, M. C.; Ross, F. M. Germanium Nanowire Growth Below the Eutectic Temperature. *Science* **2007**, *316*, 729−732.
(20) Kodambaka, S.; Hannon, J. B.; Tromp, R. M.; Ross, F. M. Control of Si Nanowire Growth by Oxygen. *Nano Lett.* **2006**, *6*, 1292−1296.
(21) Wang, L. H.; Liu, P.; Guan, P. F.; Yang, M. J.; Sun, J. L.; Cheng, Y. Q.; Hirata, A.; Zhang, Z.; Ma, E.; Chen, M. W.; Han, X. D. *In situ* Atomic-Scale Observation of Continuous and Reversible Lattice Deformation Beyond the Elastic Limit. *Nat. Commun.* **2013**, *4*, 2413.
(22) Han, X. D.; Zhang, Y. F.; Zheng, K.; Zhang, X. N.; Zhang, Z.; Hao, Y. J.; Guo, X. Y.; Yuan, J.; Wang, Z. L. Low-Temperature *in situ* Large Strain Plasticity of Ceramic Sic Nanowires and Its Atomic-Scale Mechanism. *Nano Lett.* **2007**, *7*, 452−457.
(23) McDowell, M. T.; Ryu, I.; Lee, S. W.; Wang, C. M.; Nix, W. D.; Cui, Y. Studying the Kinetics of Crystalline Silicon Nanoparticle Lithiation with *in situ* Transmission Electron Microscopy. *Adv. Mater.* **2012**, *24*, 6034−6041.
(24) Gutsche, C.; Niepelt, R.; Gnauck, M.; Lysov, A.; Prost, W.; Ronning, C.; Tegude, F. J. Direct Determination of Minority Carrier Diffusion Lengths at Axial GaAs Nanowire P-N Junctions. *Nano Lett.* **2012**, *12*, 1453−1458.
(25) Lysov, A.; Vinaji, S.; Offer, M.; Gutsche, C.; Regolin, I.; Mertin, W.; Geller, M.; Prost, W.; Bacher, G.; Tegude, F. J. Spatially Resolved Photoelectric Performance of Axial GaAs Nanowire pn-Diodes. *Nano Res.* **2011**, *4*, 987−995.
(26) Ge, S. P.; Jiang, K. L.; Lu, X. X.; Chen, Y. F.; Wang, R. M.; Fan, S. S. Orientation-Controlled Growth of Single-Crystal Silicon-Nanowire Arrays. *Adv. Mater.* **2005**, *17*, 56−61.
(27) Adhikari, H.; Marshall, A. F.; Chidsey, C. E. D.; McIntyre, P. C. Germanium Nanowire Epitaxy: Shape and Orientation Control. *Nano Lett.* **2006**, *6*, 318−323.
(28) Ihn, S. G.; Song, J. I.; Kim, T. W.; Leem, D. S.; Lee, T.; Lee, S. G.; Koh, E. K.; Song, K. Morphology- and Orientation-Controlled Gallium Arsenide Nanowires on Silicon Substrates. *Nano Lett.* **2007**, *7*, 39−44.
(29) Joyce, H. J.; Wong-Leung, J.; Gao, Q.; Tan, H. H.; Jagadish, C. Phase Perfection in Zinc Blende and Wurtzite III− V Nanowires Using Basic Growth Parameters. *Nano Lett.* **2010**, *10*, 908−915.
(30) Han, N.; Hou, J. J.; Wang, F.; Yip, S.; Lin, H.; Fang, M.; Xiu, F.; Shi, X.; Hung, T.; Ho, J. C. Large-Scale and Uniform Preparation of Pure-Phase Wurtzite GaAs NWs on Non-Crystalline Substrates. *Nanoscale Res. Lett.* **2012**, *7*, 1−6.
(31) Krogstrup, P.; Popovitz-Biro, R.; Johnson, E.; Madsen, M. H.; Nygård, J.; Shtrikman, H. Structural Phase Control in Self-Catalyzed Growth of GaAs Nanowires on Silicon (111). *Nano Lett.* **2010**, *10*, 4475−4482.
(32) Schmidt, V.; Senz, S.; Gösele, U. Diameter-Dependent Growth Direction of Epitaxial Silicon Nanowires. *Nano Lett.* **2005**, *5*, 931−935.
(33) Cai, Y.; Chan, S. K.; Soar, I. K.; Chan, Y. T.; Su, D. S.; Wang, N. The Size-Dependent Growth Direction of ZnSe Nanowires. *Adv. Mater.* **2006**, *18*, 109−114.
(34) Wu, Y.; Cui, Y.; Huynh, L.; Barrelet, C. J.; Bell, D. C.; Lieber, C. M. Controlled Growth and Structures of Molecular-Scale Silicon Nanowires. *Nano Lett.* **2004**, *4*, 433−436.
(35) Pankoke, V.; Kratzer, P.; Sakong, S. Calculation of the Diameter-Dependent Polytypism in GaAs Nanowires from an Atomic Motif Expansion of the Formation Energy. *Phys. Rev. B: Condens. Matter Mater. Phys.* **2011**, *84*, 075455.
(36) Shtrikman, H.; Popovitz-Biro, R.; Kretinin, A.; Houben, L.; Heiblum, M.; Bukała, M.; Galicka, M.; Buczko, R.; Kacman, P. Method for Suppression of Stacking Faults in Wurtzite III− V Nanowires. *Nano Lett.* **2009**, *9*, 1506−1510.
(37) Han, N.; Hou, J. J.; Wang, F. Y.; Yip, S.; Yen, Y. T.; Yang, Z. X.; Dong, G. F.; Hung, T.; Chueh, Y. L.; Ho, J. C. GaAs Nanowires: From Manipulation of Defect Formation to Controllable Electronic Transport Properties. *ACS Nano* **2013**, *7*, 9138−9146.
(38) Han, N.; Wang, F.; Hou, J. J.; Yip, S.; Lin, H.; Fang, M.; Xiu, F.; Shi, X.; Hung, T.; Ho, J. C. Manipulated Growth of GaAs Nanowires: Controllable Crystal Quality and Growth Orientations *via* a Supersaturation-Controlled Engineering Process. *Cryst. Growth Des.* **2012**, *12*, 6243−6249.
(39) Lugstein, A.; Steinmair, M.; Hyun, Y. J.; Hauer, G.; Pongratz, P.; Bertagnolli, E. Pressure-Induced Orientation Control of the Growth of Epitaxial Silicon Nanowires. *Nano Lett.* **2008**, *8*, 2310−2314.
(40) Holmes, J. D.; Johnston, K. P.; Doty, R. C.; Korgel, B. A. Control of Thickness and Orientation of Solution-Grown Silicon Nanowires. *Science* **2000**, *287*, 1471−1473.
(41) Yang, L. J.; Wang, S.; Zeng, Q. S.; Zhang, Z. Y.; Pei, T.; Li, Y.; Peng, L. M. Efficient Photovoltage Multiplication in Carbon Nanotubes. *Nat. Photonics* **2011**, *5*, 673−677.
(42) Lide, D. R. *CRC Handbook of Chemistry and Physics*; CRC Press: Boca Raton, 2010.
(43) Sandroff, C. J.; Hegde, M. S.; Farrow, L. A.; Chang, C. C.; Harbison, J. P. Electronic Passivation of GaAs-Surfaces through the Formation of Arsenic Sulfur Bonds. *Appl. Phys. Lett.* **1989**, *54*, 362−364.
(44) Léonard, F.; Talin, A. A. Electrical Contacts to One-and Two-Dimensional Nanomaterials. *Nat. Nanotechnol.* **2011**, *6*, 773−783.
(45) Hou, J. J.; Han, N.; Wang, F.; Xiu, F.; Yip, S.; Hui, A. T.; Hung, T.; Ho, J. C. Synthesis and Characterizations of Ternary InGaAs Nanowires by a Two-Step Growth Method for High-Performance Electronic Devices. *ACS Nano* **2012**, *6*, 3624−3630.

DOI: 10.1021/acsnano.6b02473
ACS Nano 2016, 10, 6283−6290